Journal of Quantitative Spectroscopy & Radiative Transfer 286 (2022) 108206

Contents lists available at ScienceDirect

Journal of Quantitative Spectroscopy & Radiative Transfer

journal homepage: www.elsevier.com/locate/jqsrt

The water vapor self-continuum absorption at room temperature in the 1.25 μm window

A.O. Koroleva[a,b], S. Kassi[a], A. Campargue[a,*]

[a] Univ Grenoble Alpes, CNRS, LIPhy, Grenoble, France
[b] Institute of Applied Physics of RAS, Nizhniy Novgorod, Russia

ARTICLE INFO

Article history:
Received 9 February 2022
Revised 11 April 2022
Accepted 11 April 2022
Available online 13 April 2022

Keywords:
Water vapor
Continuum absorption
MT_CKD model
CRDS
Atmospheric window
Water dimer

ABSTRACT

The water vapor self-continuum is newly measured at room temperature in the high energy edge of the 1.25 μm window by using highly stable and sensitive cavity ring down spectroscopy (CRDS). Self-continuum cross-sections, C_S, are derived between 8290 and 8620 cm^{-1} at 29 selected spectral points by using pressure ramps (up to 15 Torr) of pure water vapor. Purely quadratic pressure dependence is obtained for the absorption coefficient at each measurement point. Although the spectral measurement points were chosen to minimize the contribution of resonance line absorption, the latter represents between 30 and 70% of the measured absorption in the studied region. The measurements are found consistent with a previous study of the low frequency edge of the 1.25 μm windows and (Campargue et al. J Geophys Res Atmos 2016;121:13,180 – 13,203. doi:10.1002/2016JD025531). The frequency dependence of the retrieved C_S values shows an overall good agreement with the MT_CKD values, although an additional broad absorption feature is observed with a center near 8455 cm^{-1}. It is tentatively interpreted as a possible impact of the uncertainties on the resonance line contribution on the derived C_S values or as a possible evidence of a band of the bound dimers, $(H_2O)_2$.

1. Introduction

Water vapor absorption represents more than half of the solar light absorbed by the Earth atmosphere. The water absorption spectrum shows strong rovibrational bands separated by spectral regions of lower opacity, the transparency windows. The water continuum is mostly smooth and structureless and follows a frequency dependence similar to the envelope of the rovibrational spectrum. Although the continuum amplitude sharply decreases in the windows, its relative importance is much higher than in the band regions where the line absorption generally dominates.

Note that in the Earth's atmosphere, the water continuum arises from the interaction of water molecules with each other and with other atmospheric molecules (self- and foreign-continuum, respectively). In order to account for the water vapor continuum absorption in atmospheric radiative transfer codes, the semi-empirical MT_CKD model [1–3] is generally implemented. This model uses an empirical line shape modeling with sub-Lorentzian far wings and a weak interaction term between a water vapor molecule and another molecule for the intermediate wings. The parameters of this empirical line shape have been fitted to a selection of laboratory or field measurements available mostly in the mid infrared (see [2,4] and references therein).

The quantitative determination of weak absorption continua by transmission spectroscopy is generally challenging as continua show up as small decreases of the transmitted spectrum baseline when the absorption cell is filled with the studied gas species. The challenge is made particularly difficult in the case of water vapor because of possible experimental biases due to surface effects (adsorption, condensation) on the optics of the experimental setup. Since the pioneer works of Burch using a grating spectrograph in the 10 μm and 4.0 μm transparency windows [5–7], large experimental efforts have been undertaken to characterize the water self-continuum in the atmospheric windows. Room temperature measurements performed by Fourier transform spectroscopy (FTS) at RAL (Rutherford Appleton laboratory) within the frame of the CAVIAR (Continuum Absorption at Visible and Infrared wavelengths and its Atmospheric Relevance) [8] and at the Institute of Atmospheric Optics in Tomsk [9,10] were found in good agreement with each other but largely above the MT_CKD values in the 4.0, 2.1 and 1.6 μm windows. The overview comparison of the FTS self-continuum cross-sections (C_S) to the corresponding MT_CKD values between 1500 and 1000 cm^{-1} is presented in Fig. 1. The FTS cross-sections have an unexpectedly similar value in the 4.0, 2.1 and 1.6 μm windows ($C_S \approx 2 \times 10^{-23}$ cm^2 $molecule^{-1}atm^{-1}$) while

* Corresponding author.
E-mail address: Alain.Campargue@univ-grenoble-alpes.fr (A. Campargue).

https://doi.org/10.1016/j.jqsrt.2022.108206
0022-4073/

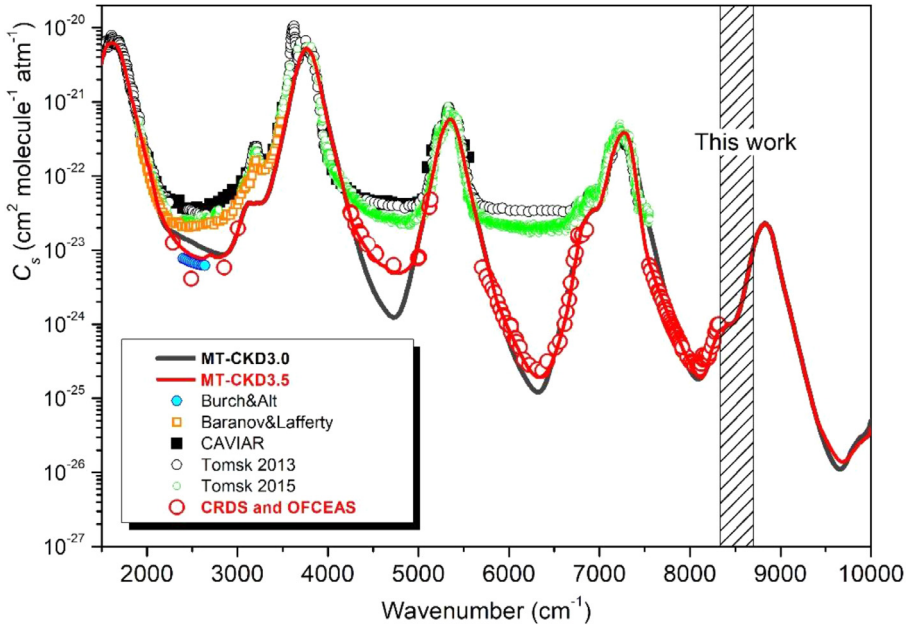

Fig. 1. Overview comparison of the self-continuum cross-section of water vapor near room temperature between 1500 and 9000 cm^{-1}. Solid lines show different versions of the MT_CKD 3.0 and 3.5 versions at 296 K [3]. Experimental results were obtained by OFCEAS and CRDS (red circles; [11–18]); by FTS from [21] (orange open squares), from CAVIAR consortium (black full squares; [8]), from Tomsk2013 (black open circles; [9]), from Tomsk2015 (green circles; [10]) and with a grating spectrograph by [6,7] (blue circles). The 8290–8620 cm^{-1} spectral interval presently studied by CRDS is indicated.

the MT_CKD values decrease significantly from the 4.0 window to the 1.6 µm window. As a result, the disagreement reaches two orders of magnitude compared to Tomsk measurements near 1.6 µm [9,10]. In the last years, we have undertaken a characterization of the self-continuum of water vapor using cavity enhanced absorption spectroscopies (CEAS) [11–18], namely cavity ring down spectroscopy (CRDS) and optical feedback–cavity enhanced absorption spectroscopy (OF-CEAS). These CEAS self-continuum absorption retrievals were all supported by a clear pressure squared dependence of the continuum absorption in order to exclude potential experimental biases. As illustrated in Fig. 1, the CEAS measurements sampling the 4.0, 2.1, 1.6 and 1.25 µm windows validate the overall frequency dependence of the MT_CKD continuum. The 3.0 version of the MT_CKD continuum, elaborated before the CEAS measurements, nevertheless showed significant deviations, by up a factor of five in the center of the 2.3 µm window. Starting from the 3.2 version, CEAS cross-sections were considered as experimental constraints of the MT_CKD continuum (see Fig. 1). Note that it appeared that the CAVIAR and Tomsk room temperature self-continuum values were affected by reflectivity issues related to the adsorption of water on the optics of the multipass cell used for the FTS recordings [19,20].

The physical origin of the water vapor continuum is one of the most long-standing issues in molecular spectroscopy. Although being mostly based on far-wing line-by-line calculations, the widely used MT_CKD continuum might account in an operative way for different contributions including not only deviations of the far wings from calculated profiles but also absorption due to metastable (quasibound) and stable (truly bound) dimers [22].

The experimental evidence of a contribution of bound water dimers (BWD, hereafter) is difficult as BWD bands are expected to show up as weak unresolved structures, generally overlapping with the wider envelope of the water monomer (WM) bands and superimposed to the far-wing continuum whose envelope resembles that of the WM resonance lines.

Based on theoretical predictions of the BWD spectrum, different spectral regions have been considered for detection of BWD spectral signatures in water vapor at thermodynamical equilibrium:

(i) Twenty years ago, on the basis of calculations by Low and Kjaergaard [23], the detection of BWD absorption was reported near 750 nm from low resolution spectra recorded in open air atmosphere with an 18.4 km absorption path length over the sea [24]. In spite of a weaker intensity of near-infrared BWD bands, the 750 nm spectral region was targeted as it limits interference with WM absorption. The claimed BWD evidence was obtained by difference of the measured atmospheric absorbance and a simulation of the WM absorption lines relying on the version of the HITRAN database available at that time. Later, a high number of weak WM lines missing in the used HITRAN list were measured by CRDS [25]. The resulting additional absorbance was found to represent an important fraction of the reported BWD atmospheric absorption and questioned the reliability of the BWD detection, which was finally revoked [26].

(ii) The mm-submm wave range where the BWD pure rotational spectrum is located, offers an alternative way to minimize the spectral interference between BWD and WM absorption. A series of thirteen quasi-equidistant spectral features recorded in water vapor at room temperature in the 0.1–0.26 THz (3.5–8.7 cm^{-1}) interval [27–29] was found in good agreement with first principle calculations of transitions computed between all rovibrational states [30]. This observation provided the first definitive detection of BWDs in equilibrium water vapor at room temperature. Moreover, BWDs were confirmed to bring the largest contribution to the room temperature continuum absorption in the considered mm-wave range.

(iii) Although the discrimination of BWD absorption in the in-band self-continuum is complicated, strong evidence of BWD signature has been reported in the monomer bending region near 1600 cm^{-1}, in the OH stretching fundamental band near 3700 cm^{-1} and in the region of the stretch-bend combination band near 5300 cm^{-1} [31–35]. Distinct (broad) spectral peaks were found to coincide with BWD calculated spectrum [23,36,37] leaving little doubt on the BWD contribution to the in-band continuum. Very recently, similar comparison between WD predicted spectrum and FTS self-continuum measurements were performed in the region of the bands at 8800

and 10,600 cm^{-1} [38]. The measurements were performed at high temperature (398 K and 431 K) in order to allow for using high water vapor pressure values (1–4 atm). A dimer-based model including both quasibound and bound WD contributions was developed and found to fit reasonably well to the measured self-continuum. About half of the measured continuum was found to have a WD origin, the quasibound contribution being larger than the BWD contribution for the considered bands [38].

The present study is devoted to the first experimental retrieval of the room temperature water vapor self-continuum in the 8290–8620 cm^{-1} spectral range, thus extending to higher energy our previous CEAS studies. The studied region corresponds to the high energy edge of the 1.25 µm window (see Fig. 1). The center and low energy range of the window (7548–8318 cm^{-1}) were previously investigated by CRDS in Ref. [12]. The characterization of the atmospheric absorbers in this particular window is of importance as the 1.27 µm oxygen band (including rovibronic lines superimposed over a broad collision induced absorption (CIA) band - see *e.g.* [39,40]) is considered for air-mass determination in a number of satellite missions [41]. In addition, near 8500 cm^{-1}, the studied region overlaps the above mentioned FTS investigation at high temperature [38] which will allow for a discussion of the temperature dependence. Finally, a BWD absorption band is predicted with significant intensity in the studied spectral interval and its detection would be the first experimental evidence of the BWD contribution to the continuum in the near infrared transparency windows.

In the following Part 2, we will present the experimental procedure and data acquisition. Part 3 is devoted to the retrieval of the cross-sections while comparison to the literature, considerations about the temperature dependence and possible detection of a BWD signature are presented in Part 4 before the concluding remarks (Part 5).

2. CRDS measurements

2.1. CRDS setup

Self-continuum measurements were performed by CRDS at a series of spectral points sampling the 8293 - 8621 cm^{-1} spectral interval. An external cavity diode laser (ECDL) was used as light source. The reader is referred to [42,43] for the description of the cavity ring down spectrometer and the frequency tuning of the ECDL. Briefly, the ECDL central emission frequency is tuned by changing the laser current together with the grating angle driven by a piezoelectric transducer (PZT). The typical mode-hop free tuning range of the ECDL used here (Toptica fiber-connected DL pro, 1200 nm) is about 0.8 cm^{-1}. The 1.40 m long CRDS cell is fitted by high reflectivity mirrors leading to ring down times of about 350 µs around 8300 cm^{-1}. The setup is fibered and the polarization is maintained up to the optical cavity, providing better reproducibility. The wavenumber of the ECDL is measured by a commercial Fizeau type wavemeter (HighFinesse WSU7-IR, 5 MHz resolution, 20 MHz accuracy over 10 h) that allows laser frequency to be determined at a typical 100 Hz refresh rate. The laser frequency was stable within 3 MHz during the short time of each recording (a few minutes).

The output mirror of the cavity is mounted on a piezoelectric transducer to periodically change the cell length allowing covering one free spectral range (FSR) of the cavity and thus achieving resonance between the laser light and one longitudinal mode of the cavity. After a build-up time necessary to fill the cavity with photons at resonance, the injection of laser light is stopped thanks to an acousto-optic modulator and the purely exponential decay time of photons leaking from the cavity (*i.e.* the ring down (RD) time, τ) is measured with a photodiode. The fitted RD time is directly related to the absorption coefficient of the absorbing gas, $\alpha(\nu)$:

$$\alpha(\upsilon) = \frac{1}{c\tau(\upsilon)} - \frac{1}{c\tau_0(\upsilon)} \quad (1)$$

where c is the speed of light, ν is the laser frequency. τ_0 and τ are the ring down time with the optical cavity empty, or filled with a non-absorbing gas, respectively.

Two pressure gauges (10 and 1000 Torr full scale, from MKS Instruments) were installed on the cavity to continuously measure the total pressure with an accuracy of 0.25% of reading. A temperature sensor (TSic 501 from IST, ±0.1 K accuracy) was fixed on the external wall of the cavity and enveloped by thermal insulation foam to continuously record the temperature which remained in the 294±1 K range during the whole measurement campaign.

2.2. Data acquisition

As described below, measurements were performed for increasing and decreasing pressure ramps at fixed frequency. We nevertheless present in Fig. 2 some spectra recorded for different pressure values in order to illustrate how the measurement spectral points were selected. Water continuum is generally much weaker than resonance line contribution, but in well-chosen microwindows of transparency, the continuum may become equivalent to the resonance line absorption or even predominant. This is illustrated in Fig. 2 in the region of the selected 8301.825 cm^{-1} measurement point (dashed vertical line). For a pressure of 8.2 Torr, the measured absorption coefficient at 8301.825 cm^{-1} involves equivalent contributions of the self-continuum and of the WM resonance lines (obtained from a spectrum simulation - see below). Note that the far-wing and the self-continuum contributions have both a pressure-squared dependence which makes their relative importance independent on the pressure. On the right panel of Fig. 2, the pressure dependence of the spectrum is illustrated for four pressure values ranging from 2.9 to 8.2 Torr. The spectrum baseline (corrected from the empty cavity loss rate) is observed to increase rapidly (in fact, quadratically) with pressure.

Twenty-nine spectral points were thus selected far from intense water vapor lines in order to reduce the impact of the uncertainty of the line parameters which is the main uncertainty source of the derived cross-sections (see below). The sensitivity of the recordings makes it necessary to consider the presence of impurities in the water sample. Indeed, NH_3 and CO_2 might be present in the sample with maximum relative abundances of 5 ppm and 120 ppm, respectively, which makes their strongest transitions observable in the region. For instance, in the region displayed in Fig. 2, a CO_2 and a NH_3 line are visible at 8301.293 cm^{-1} and 8301.756 cm^{-1}, respectively. At the chosen spectral points, the CO_2 and NH_3 line contributions are all less than 0.1% of the total absorption and can be neglected.

At the beginning of each day of measurements, the water sample was purified by cooling with liquid nitrogen and evacuating the residual vapor phase. For each selected spectral point, the absorption coefficient was recorded during an increasing pressure ramp from 0 to 15 Torr (*i.e.* about 71% of the saturation pressure at 296 K) followed by a decreasing pressure ramp. The pressure was varied at a speed of about 0.1 Torr/second in order to limit the influence of adsorption and desorption effects which become noticeable at lower speed. The typical duration of the pressure cycle was 6–7 min.

Some measurements were repeated several times to check the repeatability. The linear dependence of the absorption coefficient *versus* pressure squared is illustrated in Fig. 3 for five spectral points (Note that the residuals displayed on the figure correspond to the superposition of the five linear fits of the measurements).

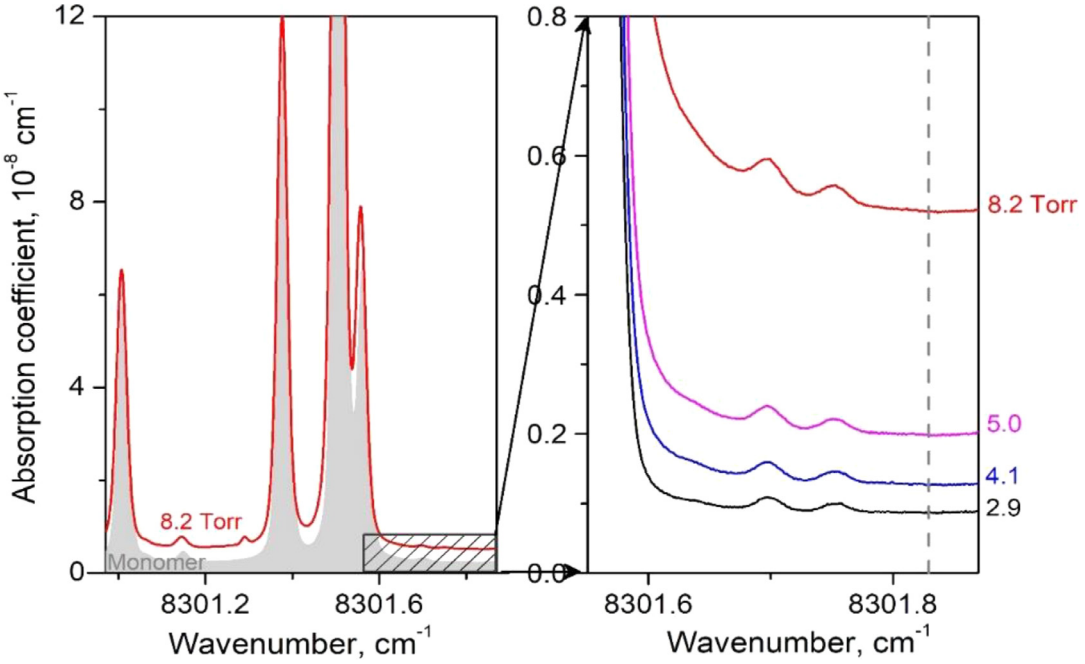

Fig. 2. *Left panel:* Comparison of the CRDS absorption coefficient for water vapor at a pressure of 8.2 Torr with a resonance line simulation modeled using HITRAN2020 [44]. The zero absorption baseline was fixed to the loss rate value obtained with an empty cavity. *Right panel:* Pressure dependence of CRDS spectra of pure water vapor near 8301 cm^{-1}, showing the increase of the baseline level due to water vapor self-continuum (the constant term due to the empty cavity losses was subtracted). The vertical dashed line corresponds to the spectral point at 8301.825 cm^{-1} selected for the continuum measurement.

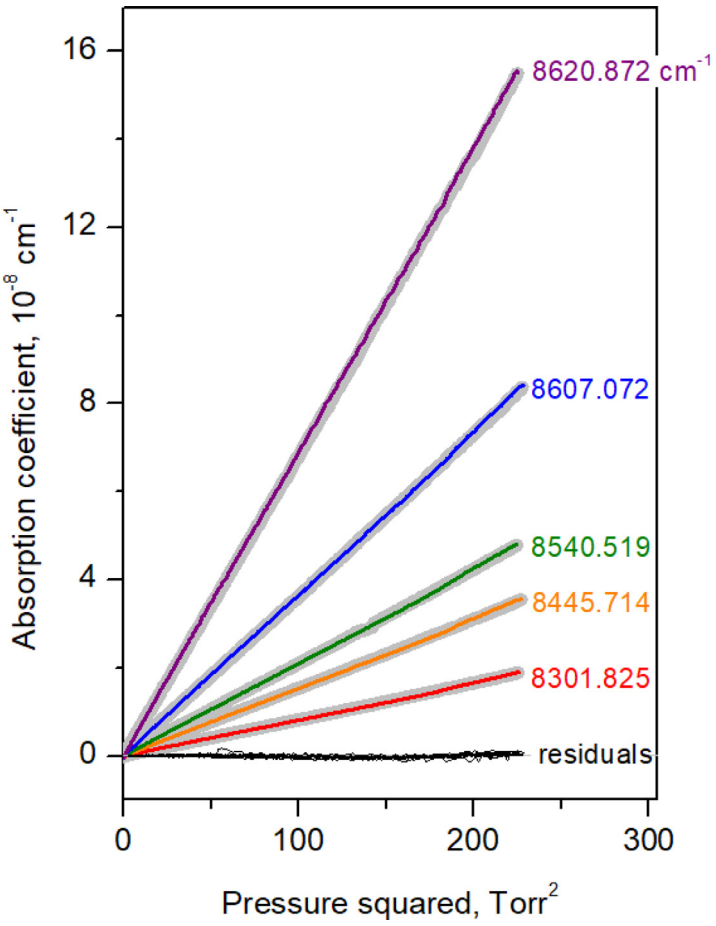

Fig. 3. Self-continuum absorption *versus* the squared water vapor pressure during pressure ramps up to 15 Torr for different spectral points of the 1.25 μm window. For each spectral point, measurements were performed during increasing and decreasing pressure ramps (gray and colored lines, respectively). The self-continuum cross-section values were derived from the linear fits. The residuals (black line) correspond to the superposition of the differences between measurements and the five linear fits.

Table 1
Self-continuum cross sections of water vapor at room temperature (294 K) derived between 8293 and 8621 cm^{-1}.

Frequency cm^{-1}	C_s[a] 10^{-24} $cm^2 molecule^{-1}$ atm^{-1}	R_{WML}[b] %	C_s Unc[c] %	Nb of ramps
8293.592	0.883(1)	29.7	12.6	1
8301.825	1.076(1)	44.0	24.3	2
8317.615	1.026(27)	42.7	22.8	3
8336.464	0.937(7)	56.8	39.7	2
8346.523	0.896(9)	45.6	20.2	2
8355.863	0.953(2)	40.3	15.7	1
8375.201	0.955(3)	46.6	21.6	1
8385.874	1.038(3)	40.5	15.5	1
8392.751	1.140(3)	42.5	16.8	1
8406.511	1.208(3)	42.5	19.2	1
8412.218	1.333(3)	63.7	40.2	2
8432.946	1.501(3)	44.3	19.2	1
8434.240	1.446(3)	41.9	15.4	1
8445.714	1.559(3)	56.8	33.0	2
8456.934	1.722(3)	66.5	51.5	1
8466.674	1.386(3)	56.3	30.8	1
8480.505	1.480(7)	39.6	16.0	2
8488.515	1.49(3)	62.2	42.6	4
8496.624	1.388(6)	41.1	17.0	2
8512.892	1.513(2)	50.6	25.3	2
8535.871	1.503(4)	43.6	19.2	1
8540.519	1.923(3)	61.0	39.2	1
8548.646	1.565(3)	34.9	13.7	2
8553.827	1.656(3)	45.2	19.9	1
8573.765	2.360(4)	58.7	32.7	1
8579.992	1.916(3)	67.9	52.7	2
8598.690	2.791(4)	38.1	14.7	1
8607.072	3.247(4)	61.9	38.2	1
8620.872	5.960(68)	62.8	41.9	3

Notes.
[a] The statistical uncertainties are given within parentheses after each *Cs* value, in the unit of the last quoted digit. They include the fit uncertainty and statistical uncertainty (for the frequencies where measurements were repeated – see last column). The uncertainties related to the resonant line subtraction are much larger and included in total uncertainties given in the "C_s Unc." column.
[b] Relative contribution of the far-wing contribution to the total measured absorption coefficient: $\alpha_{RWML} = \alpha_{WML}/(\alpha_{WML}+\alpha_{WCS})$.
[c] Total uncertainty on the retrieved C_s values (in %) mainly due to uncertainty on the (subtracted) far-wing contribution, α_{WML} (see Text).

A very good coincidence is obtained for the measurements performed during increasing and decreasing pressure ramps (gray and colored lines, respectively).

2.3. Self-continuum cross-sections retrieval

The absorption coefficient, α, as defined in Eq. (1) can be expressed as:

$$\alpha(\nu, T) = \alpha_{WML} + \alpha_{WCS} = \alpha_{WML} + \frac{1}{kT} C_S(\nu, T) P^2_{H_2O} \quad (2)$$

where k is the Boltzmann constant, α_{WML} and α_{WCS} are the contributions due to resonant lines (WML) and the water vapor self-continuum (WCS), respectively. C_S is the self-continuum cross-sections expressed in $cm^2 molecule^{-1} atm^{-1}$. Note that the Rayleigh scattering which is proportional to pressure and omitted in Eq. (2) was estimated and found negligible (at 15 Torr, Rayleigh scattering losses are less than two orders of magnitude smaller than the total absorption coefficient, α).

A simulation of the water vapor rovibrational spectrum, α_{WML}, was performed at different pressures on the basis of the HITRAN2020 line list [44], using a Voigt profile and the standard wing cut-off at 25 cm^{-1} frequency detuning from the line center (the underlying pedestal is considered as part of the continuum for easier comparison with MT_CKD and other studies). For each spectral point, the proportionality factor between α_{WML} and $P^2_{H_2O}$ was determined and subtracted from the fitted slope of the absorption coefficient *versus* $P^2_{H_2O}$ (Fig. 3). The resulting value, $\frac{1}{kT} C_S(\nu, T)$, leads to the cross-sections listed in Table 1 and presented in Fig. 4. For some spectral points, several pressure ramps (up to 4 – see Table 1) were performed and the listed C_S values and corresponding statistical error bars result from the global fit of the different recordings. The statistical error resulting of the linear fit of α *versus* $P^2_{H_2O}$ is included in Table 1.

The self-continuum cross-sections are compared to the total measured cross-sections in Fig. 4. The difference corresponds to the WM resonant lines whose relative contribution to the total absorption, $R_{WML} = \alpha_{WML}/(\alpha_{WML}+\alpha_{WCS})$, is given in Table 1 for each spectral point. Although spectral points were chosen to minimize α_{WML} as much as possible, the contribution of rovibrational lines is always important in the considered region and fluctuates between 30% and 70%, according to the spectral point. It is worth noting that, as expected, the large dispersion of the measured total cross-sections is significantly reduced after subtraction of the far-wing contributions.

While the sum of the self-continuum and resonant line contributions is known experimentally with an accuracy better than 1% (see Fig. 3) the uncertainties on the C_S values are much larger if the uncertainty related to the subtracted resonant line contribution is taken into account. This is a common situation when WM resonant lines represent a significant fraction of the measured continuum and the corresponding WM line parameters are not accurately known (see *e.g.* [45]).

The uncertainty related to the line parameters can be evaluated by propagation of the uncertainties provided by HITRAN2020 for the different line parameters. In practice, only the uncertainties on the line intensities (S) and on the self-broadening coefficients (γ_{self}) have a significant impact. We have plotted in Fig. 5 the HITRAN2020 line list with a color depending on their HITRAN error code. It appears that the error code on γ_{self} corresponds to

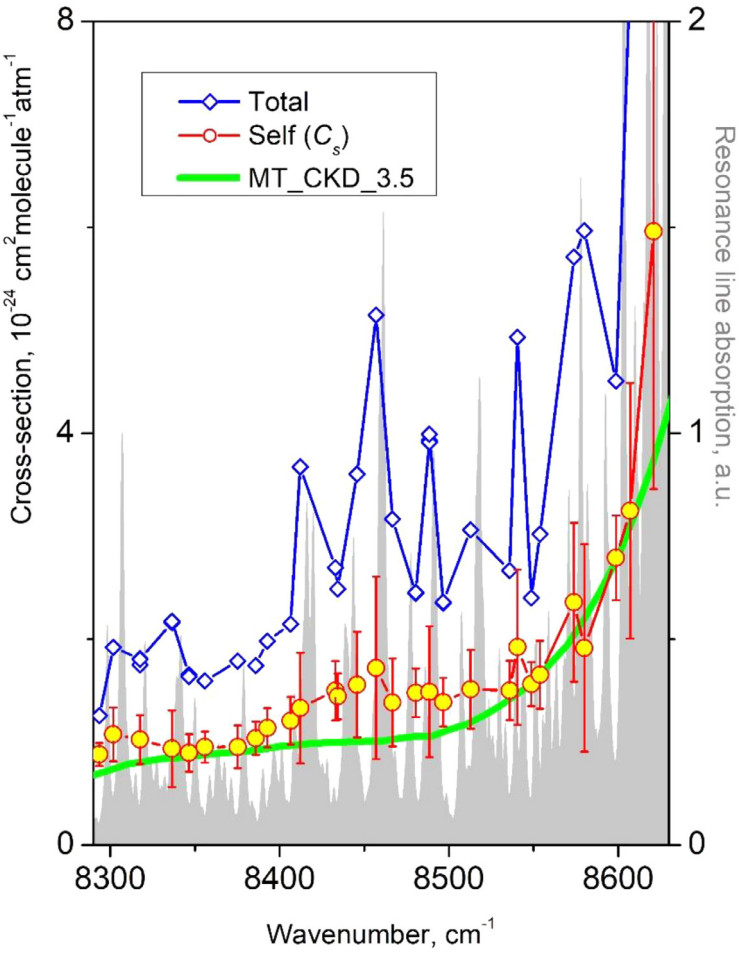

Fig. 4. Total measured cross-section of water vapor at room temperature (blue) at the measurement points selected in the 1.25 μm window. The residuals obtained after subtraction of the contribution of the resonant lines are the self-continuum absorption cross-sections (red open circles) which are plotted with their associated total error bars (dominated by the uncertainties on the resonant lines contribution). The plot includes the MT_CKD_3.5 values (green line) [3]. For comparison, a low resolution simulation of the resonance absorption cross-section is presented as gray background.

an uncertainty between 10 and 20% for most of the lines. The uncertainties on the intensities of the lines of importance are in the 5–10% and 2–5% ranges below and above 8340 cm^{-1}, respectively. As illustrated by their frequency dependence, HITRAN uncertainties should be considered as rough estimates. Considering that α_{WML} at a frequency detuned from the line center is simply proportional to γ_{self} and S, their relative uncertainties propagate unchanged on α_{WML}. Based on the above HITRAN uncertainties, we roughly take an overall (probably conservative) value of 20% for the α_{WML} uncertainty which leads to a relative error on C_S of $20\% \times R_{WML}/(1-R_{WML})$. As the R_{WML} values range between 35 and 68%, we obtain uncertainty values on C_S ranging between about 8 and 42%, typically one order of magnitude larger than the uncertainty on the measured total absorption coefficient ($\alpha_{WML}+\alpha_{WCS}$). A more rigorous treatment by propagation of the HITRAN uncertainties and taking into account of the statistical uncertainties leads to total uncertainty values ranging between 12 and 53% (see Table 1).

3. Discussion

3.1. Comparison to literature values

The retrieved C_S values listed in Table 1 are plotted in Fig. 6 together with the previous CRDS measurements below 8310 cm^{-1} [12] and compared to the MT_CKD_3.5 [3] values. It is worth mentioning that as in [12], the plotted experimental error bars do not include the uncertainty due to the resonant lines estimated above.

The first three measurement points near 8300 cm^{-1} are in common with those of Ref. [12]. The present values are larger by 6.3, 8.4 and 6.5% compared to [12]. These deviations are compatible with the combined error bars on the two C_S determinations, on the order of 5.7, 9.5 and 10.0%, respectively. Nevertheless, the agreement is in fact better than reflected by the 7% average deviation between the two determinations. Half of the disagreement is related to the different versions of the HITRAN database used to calculate the resonance line contribution, α_{WML}. As reflected by the $\alpha_{WML}/(\alpha_{WML}+\alpha_{WC})$ relative contribution values given in [12] and in Table 1 for the three measurements in common, the resonance line contributions based on HITRAN2012 are larger by about 3% compared to the present values based on the HITRAN2020 version. This example illustrates the direct correlation between the retrieved continuum cross-section values and the line list used to calculate α_{WML} in the spectral regions where WM resonance line contribution is important. In principle, published C_S values should be used with the same line list as that adopted for the C_S retrieval from the measurements.

The comparison with the MT_CKD_3.5 model shows an overall very good agreement. Below 8300 cm^{-1}, the MT_CKD model has been refined according to [12] (see Fig. 1) but above this value, the present MT_CKD_3.5 version is identical to previous versions and thus independent on our previous CEAS measurements (no other

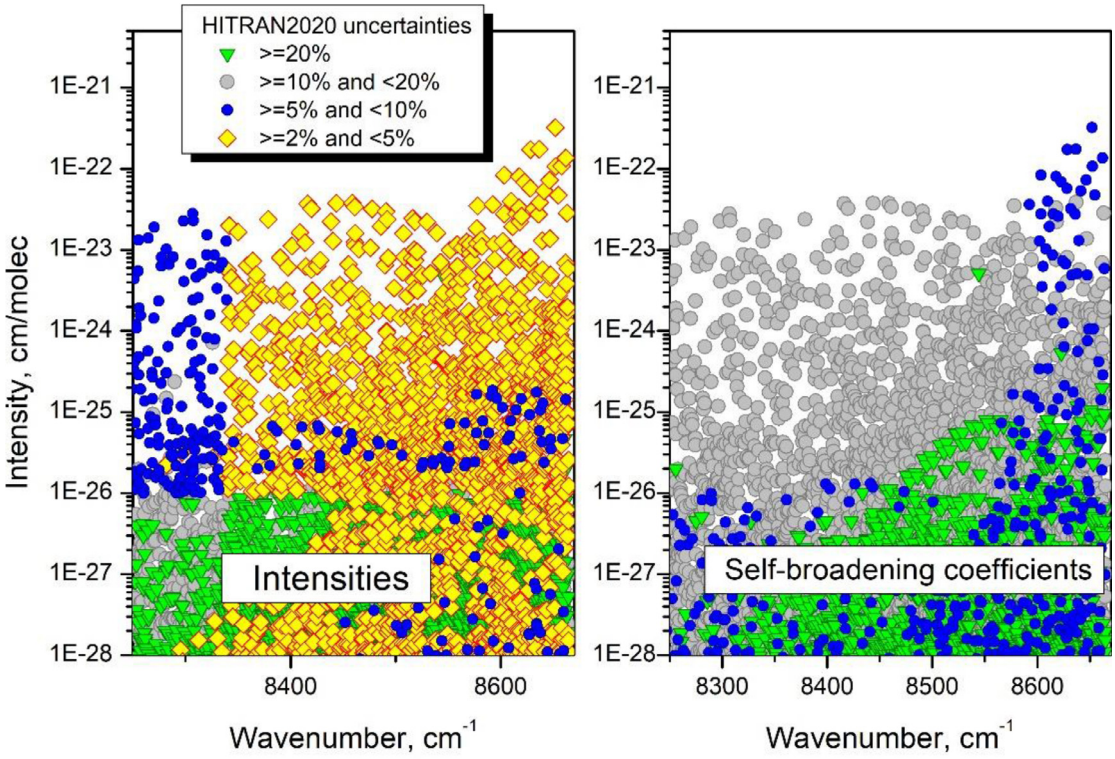

Fig. 5. Overview of the HITRAN2020 [44] line list of water vapor in the studied region with different symbols according to the error bar on the line intensities and self broadening coefficients (left and right panels, respectively).

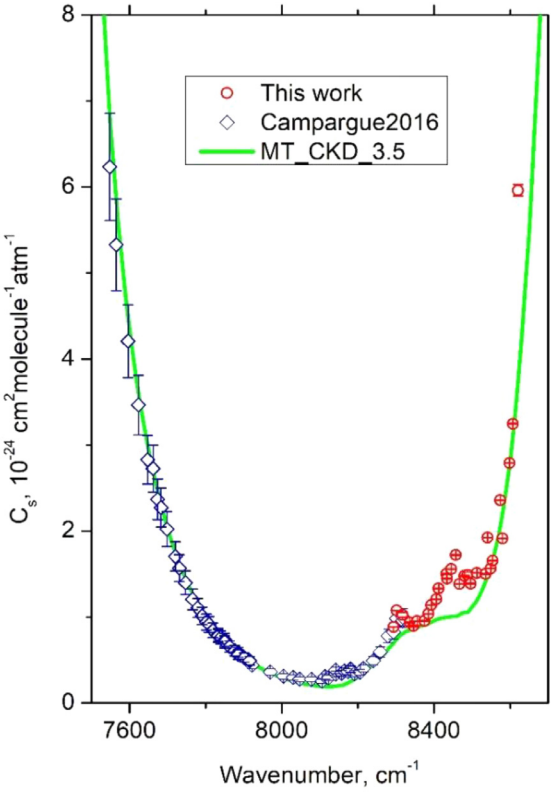

Fig. 6. Self-continuum cross-sections of water vapor at room temperature in the 1.25 μm window. The experimental values measured in [12] and in this work (blue and red circles, respectively) are compared to the MT_CKD_3.5 values. Note that the plotted error bars do not include the (large) contribution due to the resonant lines (see Table 1 and Fig. 4 for the total error bars).

room temperature measurements are available in the 1.25 µm window). The observed agreement is thus a convincing validation of the extrapolation capabilities of the MT_CKD towards high energy for practical applications.

3.2. The structure observed around 8450 cm^{-1}

The comparison to MT_CKD reveals nevertheless an additional broad structure around 8455 cm^{-1} (another weaker one seems to be present near 8300 cm^{-1}, although in coincidence with a small local maximum of the MT_CKD values). According to our evaluation of the total uncertainty of the measurement points near 8450 cm^{-1}, the observed weak structure seems to be significant (see Fig. 4). Two possible explanations are proposed for the observed structure. The first one is related to the subtraction of the resonance line contribution while the second is the possible evidence of a spectral signature of the water dimer.

The spectral measurement points around 8450 cm^{-1} correspond to a relatively large contribution of the resonance line absorption, α_{WML}, which makes the retrieved self-continuum very sensitive to the subtraction of the WM resonance lines (as reflected by the important error bars of the *Cs* values in the region- see Fig. 4). As an additional test of this sensitivity, we performed simulations of α_{WML} changing the usual ±25 cm^{-1} cut off of the plinth to ±5 cm^{-1}. This change leads to a decrease of α_{WML} and thus a general increase of the retrieved *Cs* values. In the region of interest near 8455 cm^{-1}, the resulting increase shows some faint additional structure but the scattering of the obtained *Cs* values makes it difficult to correlate with the observed structure. Let us underline that the structure was obtained following the usual ±25 cm^{-1} convention of the MT_CKD model and thus constitutes a deviation from the model, even if it is related to the resonance line subtraction.

As mentioned in the introduction, water dimers contribute to the self-continuum absorption and have been evidenced as broad spectral signatures in the near infrared in-band regions [34,35,38] and as partially resolved rotational spectrum in the mm-submm wave range [27,28]. Our tentative interpretation of the structure near 8455 cm^{-1} as a BWD band will follow the same approach based on a comparison with theory, as applied in [34,35,38,46].

By considering the dimer as two individually vibrating monomer units, Salmi et al. calculated variationally the O–H stretching vibrational overtone spectrum with a computed dipole moment surface and an internal coordinate Hamiltonian [37]. According to these calculations, a BWD band is predicted near 8530 cm^{-1}. The vibrational assignment of the BWD upper state of the band, labeled $|0>_f|2>_b|1>$ in [37], corresponds to a vibration of the donor H_2O unit of the $(H_2O)_2$ dimer, with double excitation of the bond OH stretch and a single excitation of the H_fOH_b. Although shifted by about 75 cm^{-1} from the center of the observed absorption feature, this band is the only band predicted in the region. It is located on the low energy range of a strong band system around 8800 cm^{-1} dominated by a stretch-bend band of the H_2O acceptor unit ($|20>_a|1>$ in the notation of [37]), which is predicted about 33 times stronger than the donor acceptor band near 8530 cm^{-1}.

Intensity considerations provide an additional insight. The BWD cross-section integrated over a given band is simply the product of the BWD band intensity, S_{band} in cm/molecule units, by the bond dimer equilibrium constant, K_{eq}^{b} (in atm^{-1}) (see *e.g.* Eq. (3]) in [38]):

$$\int C_S \, d\nu = K_{eq}^{b} S_{band} \tag{2}$$

According to [38], the intensity of the BWD band predicted at 8530 cm^{-1} [37], is 2.35×10^{-21} cm/molecule while the value of the equilibrium constant at room temperature is about 0.025 atm^{-1}. It leads to a calculated value of 5.87×10^{-23} cm × molecule^{-1}atm^{-1} for the integrated cross-section of the band at 8530 cm^{-1}. This value can be compared to the experimental value which is obtained from a Gaussian fit of the experimental values after subtraction of the MT_CKD baseline. An experimental value of $(4.89 \pm 1.3) \times 10^{-23}$ cm × molecule^{-1}atm^{-1} is obtained in good agreement with the predicted value, although the coincidence might be fortuitous (Note that the center and width (HWHM) values provided by the fit are 8455.2 ± 3.4 cm^{-1} and 38.4 ± 5.8 cm^{-1}, respectively).

4.3. Temperature dependence

As mentioned in the introduction, the spectral coverage of the high temperature FTS study of [38] overlaps the present measurements in the 8500–8620 cm^{-1} interval. The water vapor self-continuum is known to decrease sharply with temperature, contrary to the foreign-continuum which is much less sensitive to temperature. In the 4.0 and 2.1 µm transparency windows, the CEAS measurements near room temperature combined with high temperature CAVIAR values have provided clear evidence of a *Cs(T)* temperature dependence following a simple $\exp(\frac{D_0}{kT})$ function where D_0 is the dissociation energy of the water dimer, $D_0 = 1105(10)$ cm^{-1} [47] (see Fig. 7 of Ref. [14], Fig. 6 of [13], Fig. 6 of [17]). The situation in the 1.6 µm window is less clear, extrapolations of the high-temperature CAVIAR cross-sections leading to values larger than measured by CEAS near room temperature (see Fig. 8 in [11]).

The present room temperature cross-sections are plotted in Fig. 7 with the 398 K and 431 K values of [38] between 8475 and 8630 cm^{-1}. A third order polynomial fit of the frequency dependence of the 398 K and 431 K datasets was performed and the fitted curve was extrapolated to room temperature assuming a $\exp(\frac{D_0}{kT})$ temperature dependence. The 398 K and 431 K extrapolations are close to each other but largely above our room temperature *Cs* values (roughly by a factor of 2). Although this observation should be taken with much caution, considering the error bars of the three sets of measurements considered, the situation shows some similarity to that encountered in the 1.6 µm window [11].

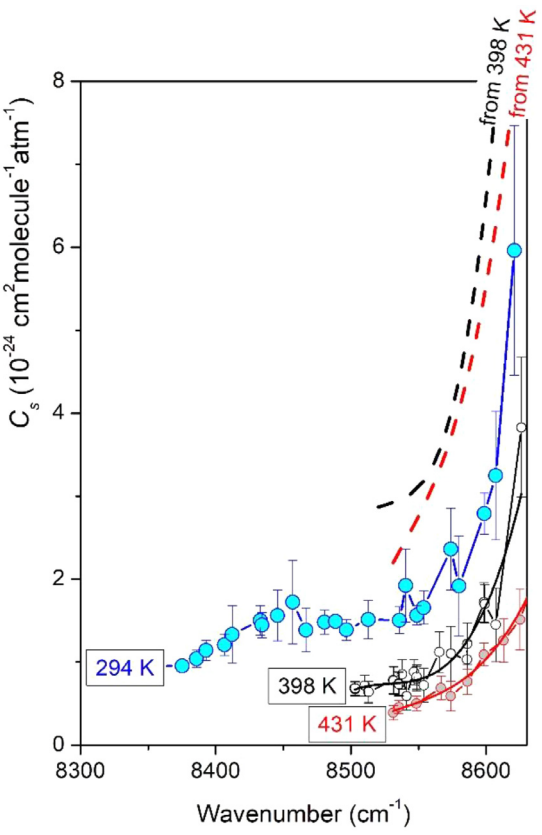

Fig. 7. Self-continuum cross-sections of water vapor between 8475 and 8630 cm^{-1} measured at room temperature (blue circles, this work) and at 398 K and 431 K [38] (black and red circles, respectively). A third order polynomial fit of the 398 K and 431 K datasets (black and red solid lines, respectively) is extrapolated to room temperature following a $\exp(\frac{D_0}{kT})$ temperature dependence datasets (black and red dashed lines, respectively). The plotted error bars include the contribution due to the resonant lines for the three datasets.

5. Conclusion

The very weak cross-sections of the water vapor self-continuum have been measured by CRDS, using pressure ramps at 29 selected spectral points of the high energy edge of the 1.25 µm window. The pure quadratic pressure dependence of the measured absorption coefficients was found to be accurately fulfilled (see Fig. 3) and coinciding results were obtained during increasing and decreasing pressure ramps. As the measured continuum includes an important contribution (30–70%) of the far-wings of the resonance lines, α_{WML}, uncertainties on the resonance line parameters directly impact the accuracy of the derived cross-sections which show a dispersion largely above the experimental accuracy of the CRDS measurements (on the order of 1%).

The measurements which are the first measurements at room temperature in the studied range, are found consistent with a previous CRDS study in the low frequency edge of the 1.25 µm window [12]. The MT_CKD model is mostly validated in the region but an additional broad absorption feature is observed with a center

near 8455 cm^{-1}. Although the observed absorption peak could be due to an inaccurate subtraction of the resonant line lines, an alternative explanation as a band of the bound dimers, $(H_2O)_2$ has been discussed. The observed peak is centered about 75 cm^{-1} above the value predicted by theoretical calculations [37]), while the band intensity is found in good coincidence with theory. If this assignment was confirmed, it would be the first experimental evidence of a $(H_2O)_2$ contribution to the water continuum in near infrared transparency. Such an interpretation is consistent with the evidence of strong $(H_2O)_2$ bands accounting for an important fraction of the continuum in the in-band regions [34,35,38] and in the rotational range [27,28].

Declaration of Competing Interest

The authors declare that they have no known competing financial interests or personal relationships that could have appeared to influence the work reported in this paper.

CRediT authorship contribution statement

A.O. Koroleva: Investigation. **S. Kassi:** Investigation. **A. Campargue:** Investigation.

Acknowledgements

This work is supported by CNRS (France) in the frame of the International Research Project “SAMIA” This work is supported by the French National Research Agency in the framework of the "Investissements d’avenir” program (ANR-15-IDEX-02).

References

[1] Clough SA, Kneizys FX, Davies RW. Line shape and the water vapor continuum. Atm Res 1989;23:229–41. doi:10.1016/0169-8095(89)90020-3.
[2] Mlawer EJ, Payne VH, Moncet J, Delamere JS, Alvarado MJ, Tobin DC. Development and recent evaluation of the MT_CKD model of continuum absorption. Phil Trans R Soc A 2012;370:2520–56. doi:10.1098/rsta.2011.0295.
[3] http://rtweb.aer.com/continuum_description.html
[4] Mlawer EJ, Turner DD, Paine SN, Palchetti L, Bianchini G, Payne VH, Cady-Pereira KE, Pernak RL, Alvarado MJ, Gombos D, Delamere JS, Mlynczak MG, Mast JC. Analysis of water vapor absorption in the far-infrared and submillimeter regions using surface radiometric measurements from extremely dry locations. J Geophys Res-Atmos 2019;124(14):8134–60 doi.org/10.1029/2018JD029508.
[5] Burch DE. Continuum absorption by H_2O, MA: Air Force Geophys Laboratory, Hanscom AFB; 1982. Report AFGL-TR-81-0300.
[6] Burch DE, Alt RL. Continuum absorption by H2O in the 700 –1200 cm^{-1} and 2400 –2800 cm^{-1} windows, MA: Air Force Geophys Laboratory, Hanscom AFB; 1984. Report AFGL-TR-84-0128.
[7] Burch DE. Absorption by H2O in narrow windows between 3000 and 4200 cm^{-1}, MA: Air Force Geophys Laboratory, Hanscom AFB; 1985. Report AFGL-TR-85-0036.
[8] Ptashnik IV, McPheat RA, Shine KP, Smith KM, Williams RG. Water vapor self-continuum absorption in near-infrared windows derived from laboratory measurements. J Geophys Res 2011;116:D16305. doi:10.1029/2011JD015603.
[9] Ptashnik IV, Petrova TM, Ponomarev YN, Shine KP, Solodov AA, Solodov AM. Near-infrared water vapor self-continuum at close to room temperature. J Quant Spectrosc Radiat Transf 2013;120:23–35. doi:10.1016/j.jqsrt.2013.02.016.
[10] Ptashnik IV, Petrova TM, Ponomarev YN, Solodov AA, Solodov AM. Water vapor continuum absorption in near-IR atmospheric windows. Atmos Oceanic Opt 2015;28:115–20. doi:10.1134/S1024856015020099.
[11] Mondelain D, Manigand S, Manigand S, Kassi S, Campargue A. Temperature dependence of the water vapor self-continuum by cavity ring-down spectroscopy in the 1.6 μm transparency window. J Geophys Res Atmos 2014;119(9):2169–8996. doi:10.1002/2013JD021319.
[12] Campargue A, Kassi S, Mondelain D, Vasilchenko S, Romanini D. Accurate laboratory determination of the near infrared water vapor self-continuum: a test of the MT_CKD model. J Geophys Res Atmos 2016;121 13,180–13,203. doi:10.1002/2016JD025531.
[13] Richard L, Vasilchenko S, Mondelain D, Ventrillard I, Romanini D, Campargue A. Water vapor self-continuum absorption measurements in the 4.0 and 2.1 μm transparency windows. J Quant Spectrosc Radiat Transf 2017;201:171–9. doi:10.1016/j.jqsrt.2017.06.037.
[14] Lechevallier L, Vasilchenko S, Grilli R, Mondelain D, Romanini D, Campargue A. The water vapor self-continuum absorption in the infrared atmospheric windows: new laser measurements near 3.3 and 2.0 μm. Atmos Meas Tech 2018;11:2159–71. doi:10.5194/amt-11-2159-2018.
[15] Mondelain D, Vasilchenko S, Čermák P, Kassi S, Campargue A. The self- and foreign-absorption continua of water vapor by cavity ring-down spectroscopy near 2.35 µm. Phys Chem Chem Phys 2015;17 17,762–17,770. doi:10.1039/c5cp01238d.
[16] Vasilchenko S, Campargue A, Kassi S, Mondelain D. The water vapor self- and foreign-continua in the 1.6 μm and 2.3 μm windows by CRDS at room temperature. J Quant Spectrosc Radiat Transf 2019;227:230–8. doi:10.1016/j.jqsrt.2019.02.01.
[17] Ventrillard I, Romanini D, Mondelain D, Campargue A. Accurate measurements and temperature dependence of the water vapor self-continuum absorption in the 2.1 μm atmospheric window. J Chem Phys 2015;143:134304. doi:10.1063/1.4931811.
[18] Fleurbaey H, Grilli R, Mondelain D, Campargue A. Measurements of the water vapor continuum absorption by OFCEAS at 3.50 µm and 2.32 µm. J Quant Spectrosc Radiat Transf 2022;278:108004. doi.org/10.1016/j.jqsrt.2021.108004.
[19] Ptashnik IV, Solodov AA, Solodov AM. FTS measurements of the water vapor continuum absorption in 2.1 μm atmospheric window. In: The XIX symposium on high resolution molecular Spectroscopy, Nizhny Novgorod; 2019 https://symp.iao.ru/files/symp/hrms/19/presentation_11485.pdf.
[20] Elsey J, Coleman MD, Gardiner TD, Menang KP, Shine KP. Atmospheric observations of the water vapor continuum in the near-infrared windows between 2500 and 6600 cm^{-1}. Atmos Meas Tech 2020;13:2335–61. doi:10.5194/amt-13-2335-2020.
[21] Baranov YI, Lafferty WJ. The water-vapor continuum and selective absorption in the 3-5 μm spectral region at temperatures from 311 to 363 K. J Quant Spectrosc Radiat Transf 2011;112:1304–13 2011. doi:10.1016/j.jqsrt.2011.01.024.
[22] Camy-Peyret C, Vigasin AA. Weakly interacting molecular pairs: unconventional absorbers of radiation in the atmosphere. Dordrecht: Kluwer Academic; 2003. (NATO ARW Proceedings Series) p. 287.
[23] Low GR, Kjaergaard HG. Calculation of OH-stretching band intensities of the water dimer and trimer. J Chem Phys 1999;110:9104. doi:10.1063/1.478832.
[24] Pfeilsticker K, Lotter A, Peters C, Bösch H. Atmospheric detection of water dimers via near-infrared absorption. Science 2003;300:2078–80. doi:10.1126/science.1082282.
[25] Kassi S, Macko P, Naumenko O, Campargue A. The absorption spectrum of water near 750 nm by CW-CRDS: contribution to the search of water dimer absorption. Phys Chem Chem Phys 2005;7:2460–7. doi:10.1039/B502172C.
[26] Lotter A. PhD thesis. Heidelberg University; 2006.
[27] MYu Tretyakov, Serov EA, Koshelev MA, Parshin VV, Krupnov AF. Water dimer rotationally resolved millimeter-wave spectrum observation at room temperature. Phys Rev Let 2013;110:093001. http://doi.org/10.1103/PhysRevLett.110093001.
[28] Serov EA, Koshelev MA, Odintsova TA, Parshin VV, Myu Tretyakov. Rotationally resolved water dimer spectra in atmospheric air and pure water vapor in the 188–258 GHz range. Phys Chem Chem Phys 2014;16:26221 http://doi.org/10.1039/c4cp03252g.
[29] Koshelev MA, Leonov II, Serov EA, Chernova AI, Balashov AA, Bubnov GM, AF An- driyanov, Shkaev AP, Parshin VV, Krupnov AF, Tretyakov MY. New fron- tiers in modern resonator spectroscopy. IEEE Trans Terahertz Sci Technol 2018;8:773–83. doi:10.1109/TTHZ.2018.2875450.
[30] Scribano Y, Leforestier C. Contribution of water dimer absorption to the millimeter and far infrared atmospheric water continuum. J Chem Phys 2007;126:234301. http://doi.org/10.1063/1.2746038.
[31] Ptashnik I, Smith K, Shine K, Newnham D. Laboratory measurements of water vapor continuum absorption in spectral region 5000 –5600 cm^{-1}: evidence for water dimers. Q J R Meteorol Soc 2004;130:2391–408. doi:10.1256/qj.03.178.
[32] Paynter D, Ptashnik I, Shine K, Smith K. Pure water vapor continuum measurements between 3100 and 4400 cm^{-1}: evidence for water dimer absorption in near atmospheric conditions. Geophys Res Lett 2007;34:L12808 doi: 10.1029/2007GL029259.
[33] Ptashnik IV. Evidence for the contribution of water dimers to the near-IR water vapor self-continuum. J Quant Spectrosc Radiat Transf 2008;109:831–52 doi: 10.1016/j.jqsrt.20 07.09.0 04.
[34] Ptashnik I, Shine KP, Vigasin AA. Water vapor self-continuum and water dimers: 1. Analysis of recent work. J Quant Spectrosc Radiat Transf 2011;112:1286–303. doi:10.1016/j.jqsrt.2011.01.012.
[35] Birk M, Wagner G, Loos J, Shine KP. 3 μm Water vapor self- and foreign- continuum: new method for determination and new insights into the self- continuum. J Quant Spectrosc Radiat Transf 2020;253:107134. doi:10.1016/j.jqsrt.2020.107134.
[36] Schofield DP, Kjaergaard HG. Calculated OH-stretching and HOH-bending vibrational transitions in the water dimer. Phys Chem Chem Phys 2003;5 310 0–5. doi:10.1039/b304952c.
[37] Salmi T, Hänninen V, Garden AL, Kjaergaard HG, Tennyson J, Halonen L. Calculation of the O - H stretching vibrational overtone spectrum of the water dimer. J Phys Chem A 2008;112:6305–12 Correction to “Calculation of the O_H Stretching Vibrational Overtone Spectrum of the Water Dimer”. J Phys Chem A 2008; 112:6305-6312. DOI: 10.1021/jp800754y |J Phys Chem A 2012;116:796–797. dx.doi.org/10.1021/jp210675h. doi:10.1021/jp800754y.
[38] Simonova AA, Ptashnik IV, Elsey J, McPheat RA, Shine KP, Smith KM. Water vapor self-continuum in near-visible IR absorption bands: measurements and semiempirical model of water dimer absorption. J Quant Spectrosc Radiat Transf 2022;277:107957. doi:10.1016/j.jqsrt.2021.107957.

[39] Leshchishina O, Kassi S, Gordon IE, Rothman RL, Wang L, Campargue A. High sensitivity CRDS of the a1Δg-X3Σg-0-0 band of oxygen near 1.27 μm: extended observations, quadrupole transitions, hot bands and minor isotopologues. J Quant Spectrosc Radiat Transf 2010;111:2236–45. doi:10.1016/j.jqsrt.2010.05.014.

[40] Mondelain D, Kassi S, Campargue A. Accurate laboratory measurement of the O2 collision-induced absorption band Near 1.27 μm. J Geophys Res Atmos 2019;124:414–23. doi:10.1029/2018JD029317.

[41] Mendonca J, Strong K, Wunch D, Toon GC, Long DA, Hodges JT, et al. Using a speed-dependent Voigt line shape to retrieve O2 from total carbon column observing network solar spectra to improve measurements of XCO2. Atmos Meas Tech 2019;12:35–50.

[42] Kassi S, Campargue A. Cavity ring down spectroscopy with 5×10^{-13} cm^{-1} sensitivity. J Chem Phys 2012;137:234201. doi:10.1063/1.4769974.

[43] Konefał M, Mondelain D, Kassi S, Campargue A. High sensitivity spectroscopy of the O_2 band at 1.27 μm: (I) pure O_2 line parameters above 7920 cm^{-1}. J Quant Spectrosc Radiat Transf 2020;241:106653. doi:10.1016/j.jqsrt.2019.106653.

[44] Gordon IE, Rothman LS, Hargreaves RJ, Hashemi R, Karlovets EV, Skinner FM, et al. The HITRAN2020 molecular spectroscopic database. J Quant Spectrosc Radiat Transf 2022;277:107949. doi:10.1016/j.jqsrt.2021.107949.

[45] Koroleva AO, Odintsova TA, Tretyakov MY, Pirali O, Campargue A. The foreign-continuum absorption of water vapor in the far-infrared (50–500 cm^{-1}). J Quant Spectrosc Radiat Transf 2021;261:107486. doi.org/10.1016/j.jqsrt.2020.107486.

[46] Ptashnik IV, Klimeshina TE, Solodov AA, Vigasin AA. Spectral composition of the water vapor self-continuum absorption within 2.7 and 6.25 μm bands. J Quant Spectrosc Radiat Transf 2019;228:97–105. doi:10.1016/j.jqsrt.2019.02.024.

[47] Rocher-Casterline BE, Ch'ng LC, Mollner AK, Reisler H. Determination of the bond dissociation energy (D_0) of the water dimer, $(H_2O)_2$, by velocity map imaging. J Chem Phys 2011;134:211101. doi:10.1063/1.3598339.